

Systematic approach to complex periodic vortex and helix lattices

Julian Becker,* Patrick Rose, Martin Boguslawski,
and Cornelia Denz

*Institut für Angewandte Physik and Center for Nonlinear Science (CeNoS),
Westfälische Wilhelms-Universität Münster, Correnstr. 2/4, 48149 Münster, Germany*

[*julian.becker@uni-muenster.de](mailto:julian.becker@uni-muenster.de)

Abstract: We present a general comprehensive framework for the description of symmetries of complex light fields, facilitating the construction of sophisticated periodic structures carrying phase dislocations. In particular, we demonstrate the derivation of all three fundamental two-dimensional vortex lattices based on vortices of triangular, quadratic, and hexagonal shape, respectively. We show that these patterns represent the foundation of complex three-dimensional lattices with outstanding helical intensity distributions which suggest valuable applications in holographic lithography. This systematic approach is substantiated by a comparative study of corresponding numerically calculated and experimentally realized complex intensity and phase distributions.

© 2011 Optical Society of America

OCIS codes: (050.4865) Optical vortices; (090.0090) Holography; (160.1585) Chiral media;
(220.4000) Microstructure fabrication.

References and links

1. M. Decker, M. Ruther, C. E. Kriegler, J. Zhou, C. M. Soukoulis, S. Linden, and M. Wegener, "Strong optical activity from twisted-cross photonic metamaterials," *Opt. Lett.* **34**, 2501–2503 (2009).
2. S. T. Chui, "Giant wave rotation for small helical structures," *J. Appl. Phys.* **104**, 013904 (2008).
3. K. Konishi, B. Bai, X. Meng, P. Karvinen, J. Turunen, Y. P. Svirko, and M. Kuwata-Gonokami, "Observation of extraordinary optical activity in planar chiral photonic crystals," *Opt. Express* **16**, 7189–7196 (2008).
4. F. Miyamaru and M. Hangyo, "Strong optical activity in chiral metamaterials of metal screw hole arrays," *Appl. Phys. Lett.* **89**, 211105 (2006).
5. M. Thiel, G. von Freymann, and M. Wegener, "Layer-by-layer three-dimensional chiral photonic crystals," *Opt. Lett.* **32**, 2547–2549 (2007).
6. D.-H. Kwon, P. L. Werner, and D. H. Werner, "Optical planar chiral metamaterial designs for strong circular dichroism and polarization rotation," *Opt. Express* **16**, 11802–11807 (2008).
7. M. Decker, R. Zhao, C. M. Soukoulis, S. Linden, and M. Wegener, "Twisted split-ring-resonator photonic metamaterial with huge optical activity," *Opt. Lett.* **35**, 1593–1595 (2010).
8. M. Thiel, M. Decker, M. Deubel, M. Wegener, S. Linden, and G. von Freymann, "Polarization Stop Bands in Chiral Polymeric Three-Dimensional Photonic Crystals," *Adv. Mater.* **19**, 207–210 (2007).
9. J. B. Pendry, "A chiral route to negative refraction," *Science* **306**, 1353–1355 (2004).
10. C. Zhang and T. J. Cui, "Negative reflections of electromagnetic waves in a strong chiral medium," *Applied Physics Letters* **91**, 194101 (2007).
11. E. Plum, J. Zhou, J. Dong, V. Fedotov, T. Koschny, C. Soukoulis, and N. Zheludev, "Metamaterial with negative index due to chirality," *Physical Review B* **79**, 035407 (2009).
12. S. Zhang, Y.-S. Park, J. Li, X. Lu, W. Zhang, and X. Zhang, "Negative Refractive Index in Chiral Metamaterials," *Phys. Rev. Lett.* **102**, 023901 (2009).
13. M. Matuszewski, I. L. Garanovich, and A. A. Sukhorukov, "Light bullets in nonlinear periodically curved waveguide arrays," *Phys. Rev. A* **81**, 043833 (2010).
14. M. Thiel, M. Decker, M. Deubel, M. Wegener, S. Linden, and G. von Freymann, "Polarization Stop Bands in Chiral Polymeric Three-Dimensional Photonic Crystals," *Adv. Mater.* **19**, 207–210 (2007).

15. M. Thiel, H. Fischer, G. von Freymann, and M. Wegener, "Three-dimensional chiral photonic superlattices," *Opt. Lett.* **35**, 166–168 (2010).
16. C. Lu and R. Lipson, "Interference lithography: a powerful tool for fabricating periodic structures," *Laser Photon. Rev.* **4**, 568–580 (2009).
17. J. Durnin, "Exact solutions for nondiffracting beams. I. The scalar theory," *J. Opt. Soc. Am. A* **4**, 651–654 (1987).
18. E. Betzig, "Sparse and composite coherent lattices," *Phys. Rev. A* **71**, 063406 (2005).
19. A. Schinzel, "Sur l'existence d'un cercle passant par un nombre donné de points aux coordonnées entières," *Enseign. Math.* **4**, 71–72 (1958).
20. D. S. Rokhsar, D. C. Wright, and N. D. Mermin, "The two-dimensional quasicrystallographic space groups with rotational symmetries less than 23-fold," *Acta Crystallogr.* **44**, 197–211 (1988).
21. D. Rokhsar, D. Wright, and N. Mermin, "Scale equivalence of quasicrystallographic space groups," *Phys. Rev. B* **37**, 8145–8149 (1988).
22. D. Rabson, N. Mermin, D. Rokhsar, and D. Wright, "The space groups of axial crystals and quasicrystals," *Rev. Mod. Phys.* **63**, 699–733 (1991).
23. N. Mermin, "The space groups of icosahedral quasicrystals and cubic, orthorhombic, monoclinic, and triclinic crystals," *Rev. Mod. Phys.* **64**, 3–49 (1992).
24. R. N. Bracewell, *The Fourier Transform and Its Applications* (McGraw-Hill, 2000), chap. 6, pp. 105–135, 3rd ed.
25. A. König and N. D. Mermin, "Symmetry, extinctions, and band sticking," *Am. J. Phys.* **68**, 525–530 (2000).
26. C. Guo, Y. Zhang, Y. Han, J. Ding, and H. Wang, "Generation of optical vortices with arbitrary shape and array via helical phase spatial filtering," *Opt. Commun.* **259**, 449–454 (2006).
27. B. Terhalle, D. Göries, T. Richter, P. Rose, A. S. Desyatnikov, F. Kaiser, and C. Denz, "Anisotropy-controlled topological stability of discrete vortex solitons in optically induced photonic lattices," *Opt. Lett.* **35**, 604–606 (2010).
28. M. Petrović, M. Belić, C. Denz, and Y. Kivshar, "Counterpropagating optical beams and solitons," *Laser Photon. Rev.* **5**, 214–233 (2011).
29. G. Juzeliūnas and P. Öhberg, "Optical Manipulation of Ultracold Atoms," in *Structured Light and Its Applications*, D. Andrews, ed., (Elsevier, 2008), chap. 12, pp. 259–333.
30. J. Curtis, "Dynamic holographic optical tweezers," *Opt. Commun.* **207**, 169–175 (2002).
31. D. G. Grier, "A revolution in optical manipulation," *Nature* **424**, 810–816 (2003).
32. C. H. J. Schmitz, K. Uhrig, J. P. Spatz, and J. E. Curtis, "Tuning the orbital angular momentum in optical vortex beams," *Opt. Express* **14**, 6604–6612 (2006).
33. J. E. Curtis and D. G. Grier, "Modulated optical vortices," *Opt. Lett.* **28**, 872–874 (2003).
34. J. Lin, X.-C. Yuan, S. H. Tao, X. Peng, and H. B. Niu, "Deterministic approach to the generation of modified helical beams for optical manipulation," *Opt. Express* **13**, 3862–3867 (2005).
35. M. Mazilu, D. Stevenson, F. Gunn-Moore, and K. Dholakia, "Light beats the spread: non-diffracting beams," *Laser Photon. Rev.* **4**, 529–547 (2009).
36. F. Courvoisier, P.-A. Lacourt, M. Jacquot, M. K. Bhuyan, L. Furfarò, and J. M. Dudley, "Surface nanoprocessing with nondiffracting femtosecond Bessel beams," *Opt. Lett.* **34**, 3163–3165 (2009).
37. F. O. Fahrbach, P. Simon, and A. Rohrbach, "Microscopy with self-reconstructing beams," *Nat. Photonics* **4**, 780–785 (2010).
38. A. König and N. D. Mermin, "Screw rotations and glide mirrors: crystallography in Fourier space," *Proc. Natl. Acad. Sci. U.S.A.* **96**, 3502–3506 (1999).
39. B. Schaefer, E. Collett, R. Smyth, D. Barrett, and B. Fraher, "Measuring the Stokes polarization parameters," *Am. J. Phys.* **75**, 163–168 (2007).
40. J. Xavier, M. Boguslawski, P. Rose, J. Joseph, and C. Denz, "Reconfigurable optically induced quasicrystallographic three-dimensional complex nonlinear photonic lattice structures," *Adv. Mater.* **22**, 356–360 (2010).
41. X. Xiong, X. Chen, M. Wang, R. Peng, and D. Shu, "Optically nonactive assorted helix array with interchangeable magnetic / electric resonance," *Appl. Phys. Lett.* **98**, 071901 (2011).

1. Introduction

Periodic topologies and lattices of all kinds are the key ingredient in many physical systems and are increasingly attracting interest recently, since the prospects of photonic crystals and metamaterials are exceeding all expectations. In particular, arrangements with helices and strongly chiral characteristics are currently receiving more and more attention in different areas of physics, giving rise to strong optical activity [1–4], circular dichroism [1, 5–7], polarization stop bands [8], or even negative refraction [9–12]. Finally, periodically curved waveguide arrays have also been predicted to be an appropriate carrier medium for optical bullets [13].

While the benefits of chiral structures are already an undoubted fact, the quest is still open

for rapid and versatile large-area fabrication techniques. Often one resorts to time consuming direct laser writing [5, 14, 15] or electron beam lithography [1]. Meanwhile, holographic approaches [16] allow both for optimization in size and speed and are thus certainly more convenient. However, the manufacture of spiraling structures or other sophisticated arrangements by holographic means is not straightforward.

Accordingly, the goal of this paper is twofold. On the one hand, we aim to provide a framework in order to investigate the prospects and limits in the construction of periodic light fields and clarify how symmetry constraints can be accounted for. On the other hand, we elaborate how the application of these concepts brings about a multitude of fascinating lattices of interest: nondiffracting vortex beams as well as three dimensional light fields equipped with helical lines of highest intensity in chiral and achiral configurations.

This paper is organized as follows: First of all, we develop the theoretical foundation of plane-wave interference and a condition for periodicity in Section 2. Thereon, in Section 3, a framework is presented that allows for a convenient description of the symmetries of the complex interference field alongside its intensity. To elucidate these concepts, a detailed construction of nondiffracting vortex beams on a square and hexagonal lattice is provided in Section 4. After introducing our experimental setup in Section 5, we finally extend the found two-dimensional vortex lattices to their three-dimensional counterparts which leads us to complex intensity helix lattices in Section 6.

2. Periodic interference

Let us start with the fact that periodic functions in direct space have their corresponding Fourier coefficients sharply located in reciprocal space. For periodic interference in general, it will thus suffice to consider the superposition of N plane waves E_n . We restrict our analysis to $N < \infty$ and monochromatic fields. Each of these waves E_n – propagating in direction \mathbf{k}_n with real amplitude $A_n > 0$ and phase offset ψ_n – can be expressed in scalar approximation as

$$E_n = A_n e^{i\mathbf{k}_n \cdot \mathbf{r} + i\psi_n}, \quad n = 1, \dots, N. \quad (1)$$

The harmonic time dependence $e^{i\omega t}$, with $\omega = 2\pi c/\lambda$, is implicitly assumed, but neglected in notation, since only one wavelength λ is considered. This restricts the wave vectors \mathbf{k}_n to a sphere of radius $k := \|\mathbf{k}_n\| = 2\pi/\lambda \forall n$ in Fourier space.

The intensity distribution $I(\mathbf{r})$ of the superposition of all N waves is obtained as

$$I(\mathbf{r}) = \sum_{n=1}^N A_n^2 + 2 \sum_{n=2}^N \sum_{m=1}^{n-1} A_n A_m \cos(\mathbf{K}_{nm} \cdot \mathbf{r} + \Psi_{nm}), \quad (2)$$

having introduced $\mathbf{K}_{nm} = \mathbf{k}_n - \mathbf{k}_m$ as well as $\Psi_{nm} = \psi_n - \psi_m$.

Then, for monochromatic interference the most general condition in order to have a periodic (or quasiperiodic) intensity modulation in real space is that the Fourier components of the field have to be located on the intersections of the sphere of radius k with the sites of some periodic (or quasiperiodic) reciprocal lattice. For simplicity, we restrict our considerations to periodic lattices. This criterion, as simple and self-evident as it may sound, is nonetheless not very well known and does not seem to have been exploited to its full extent. Therefore, we will demonstrate its power by giving a general procedure for the construction of periodic nondiffracting beams.

By nondiffracting beam we denote a light field whose intensity distribution is invariant along one spatial direction. In the case of monochromatic interference, this can be accomplished by restricting the field's Fourier components to a circle [17]. We call the plane of this circle the transverse plane and the direction perpendicular to it the optical axis.

According to this geometry, we perform a decomposition of the wave vectors $\mathbf{k}_n = \mathbf{k}_n^\perp + \mathbf{k}_n^\parallel$ into a transverse part \mathbf{k}_n^\perp and a longitudinal one, parallel to the optical axis \mathbf{k}_n^\parallel . Since per construction all \mathbf{k}_n^\parallel are equal, only the transverse part \mathbf{k}_n^\perp is of concern.

Suppose we want the transverse field in real space to be periodic on a lattice with the basis $\mathcal{A} = \{\mathbf{a}_1, \mathbf{a}_2\}$. The reciprocal basis $\mathcal{B} = \{\mathbf{b}_1, \mathbf{b}_2\}$ is then obtained in matrix notation through

$$B = 2\pi(A^{-1})^T, \quad (3)$$

where the n -th columns of the matrices A and B are the corresponding n -th basis vectors of \mathcal{A} and \mathcal{B} . The transverse wave vectors can be cast into the form

$$\mathbf{k}_n^\perp = \mathbf{k}_0^\perp + B\mathbf{h}_n, \quad n = 1, 2 \quad (4)$$

with integer vectors \mathbf{h}_n , because every \mathbf{k}_n^\perp has to point to a site of the reciprocal lattice, and we are free to choose any linearly independent $\mathbf{h}_n \in \mathbb{Z}^2$. This choice is what determines the radius of the circle in Fourier space, namely $k^\perp := \|\mathbf{k}_n^\perp\|$. If we now put the \mathbf{h}_n together as the columns of a matrix H , we can construct the circle through the three points at $\mathbf{k}_0^\perp, \mathbf{k}_1^\perp, \mathbf{k}_2^\perp$ and in addition find the expression (using Eq. (2) with the constraint $k^\perp = \|\mathbf{k}_n^\perp\|$)

$$\mathbf{k}_0^\perp = -\frac{1}{4\pi} A(H^{-1})^T \boldsymbol{\beta}, \quad \beta_n := \|B\mathbf{h}_n\|^2. \quad (5)$$

We have thus determined the three wave vectors \mathbf{k}_n^\perp , each of which points to a reciprocal lattice site. However, depending on the initial choice of H , there may be more than three sites of intersection of the constructed circle with the lattice, i.e. solutions for \mathbf{k}_n^\perp of Eq. (4) under the constraint $\|\mathbf{k}_n^\perp\| = k^\perp$. The additional $\mathbf{k}_n^\perp = \mathbf{k}_0^\perp + B\mathbf{h}_n$, with $n > 2$, can be added to the overall light field, without the field losing its periodicity in the selected basis.

This methodology goes beyond the scheme of [18] in the sense, that the difference of two wave vectors can also be a nontrivial integral linear combination of the reciprocal basis vectors. For example, consider the lattice presented in Fig. 1(a) and 1(b). Here we have

$$\begin{aligned} \mathbf{k}_1^\perp &= \mathbf{k}_0^\perp + 2\mathbf{b}_1 - 8\mathbf{b}_2, \\ \mathbf{k}_2^\perp &= \mathbf{k}_0^\perp + 2\mathbf{b}_1 + 8\mathbf{b}_2, \\ \mathbf{k}_3^\perp &= \mathbf{k}_0^\perp + 5\mathbf{b}_1 - 5\mathbf{b}_2, \\ \mathbf{k}_4^\perp &= \mathbf{k}_0^\perp + 5\mathbf{b}_1 + 5\mathbf{b}_2. \end{aligned}$$

It was constructed in the following way (cf. Fig. 1): We start with the basis vectors $\mathbf{a}_1 = a\mathbf{e}_x$, $\mathbf{a}_2 = 3a\mathbf{e}_y$ (a being the lattice parameter), which gives the reciprocal basis as $\{\mathbf{b}_1 = (2\pi/a)\mathbf{e}_x, \mathbf{b}_2 = (2\pi/(3a))\mathbf{e}_y\}$. We choose $\mathbf{h}_1 = [2, -8]^T$, $\mathbf{h}_2 = [2, 8]^T$ and using Eqs. (4) and (5), we construct the first wave vectors

$$\begin{aligned} \mathbf{k}_0^\perp &= -\frac{50\pi}{9a}\mathbf{e}_x, \\ \mathbf{k}_1^\perp &= \mathbf{k}_0^\perp + 2\mathbf{b}_1 - 8\mathbf{b}_2 = -\frac{\pi}{9a}[14\mathbf{e}_x + 48\mathbf{e}_y], \\ \mathbf{k}_2^\perp &= \mathbf{k}_0^\perp + 2\mathbf{b}_1 + 8\mathbf{b}_2 = -\frac{\pi}{9a}[14\mathbf{e}_x - 48\mathbf{e}_y]. \end{aligned}$$

When constructing the corresponding circle (which happens to be a particular case of a Schinzel circle [19]), we realize that there are another two lattice sites on its circumference, pointed to by the wave vectors $\mathbf{k}_{3,4}^\perp = \mathbf{k}_0^\perp + B[5, \pm 5]^T$, which we add to the field. Setting all amplitudes $A_n = 1$ and setting all relative phases $\psi_n = 0$, the intensity distribution of Fig. 1(b) is obtained.

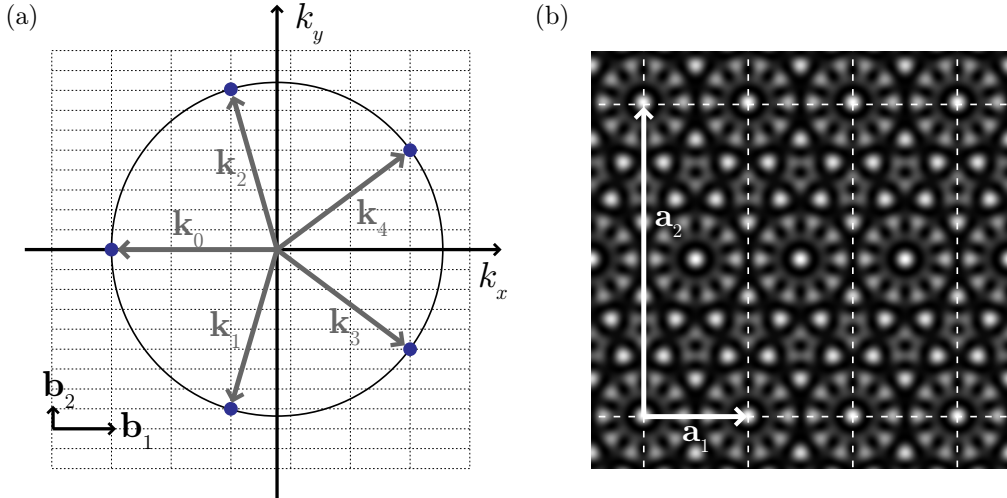


Fig. 1. Lattice given by the interference of five plane waves. (a) Fourier components of the field as points of intersection of a circle with the reciprocal lattice. (b) Numerically calculated intensity distribution in the transverse plane with the desired periodicity.

3. Symmetry considerations

Since we are using a Fourier space approach to construct our lattices, it is also adequate to describe their symmetries in terms of the Fourier coefficients of the complex field or the intensity. A suitable methodology has been supplied by Rokhsar, Wright and Mermin (RWM) [20–23], which can be used directly to describe the symmetries of the intensity in Fourier space.

Often, one is interested in the generation of intensity patterns only. However, as far as the Fourier synthesis of new lattices is concerned, it is not straightforward to control the Fourier components of the intensity. Instead, the wave vectors and phases of the fields are manipulated. Consequently, we will broaden the framework of RWM to the description of complex fields.

Considering the symmetries, there is typically no need to discriminate between two fields $E'(\mathbf{r}) = E(\mathbf{r} + \mathbf{T})$ related by a simple translation by \mathbf{T} in real space, which in Fourier space simply results in an additional linear phase factor $e^{-i\mathbf{k}\cdot\mathbf{T}}$ due to the shift theorem [24]. Also, since the fields considered here are rapidly oscillating in time, another constant phase offset $e^{i2\pi\chi_0}$, can be neglected as well. Thus, we call any two fields indistinguishable, if they can be generally related by

$$E'(\mathbf{k}) = e^{i2\pi(\chi(\mathbf{k}-\mathbf{k}_0)+\chi_0)}E(\mathbf{k}), \quad (6)$$

for any fixed \mathbf{k}_0 satisfying $E(\mathbf{k}_0) \neq 0$ (making $\mathbf{K} := \mathbf{k} - \mathbf{k}_0$ a reciprocal lattice vector) and with the so-called gauge function $\chi(\mathbf{K})$, which is linear on the lattice, i.e. if $\mathbf{b}_i, i = 1, 2, 3$ are a basis of the reciprocal lattice

$$\chi\left(\sum_i h_i \mathbf{b}_i\right) = \sum_i h_i \chi(\mathbf{b}_i) \quad \forall h_i \in \mathbb{Z}.$$

We can now define the point group G_E of the complex field as the set of all proper and improper rotations g , leaving the field unchanged modulo a gauge transformation of Eq. (6) and call the corresponding special gauge function $\Phi_g(\mathbf{K}) + \varphi_g$ a phase function of the symmetry element g :

$$E(g\mathbf{k}) = e^{i2\pi[\Phi_g(\mathbf{k}-\mathbf{k}_0)+\varphi_g]}E(\mathbf{k}). \quad (7)$$

If now $\Phi'_g(\mathbf{K}) + \varphi'_g$ is the phase function belonging to the field $E'(\mathbf{k})$ in another gauge, one can

easily see, that it is related to $\Phi_g(\mathbf{K}) + \varphi_g$ by the transformation

$$\Phi'_g(\mathbf{k} - \mathbf{k}_0) + \varphi'_g \equiv \Phi_g(\mathbf{k} - \mathbf{k}_0) + \varphi_g + \chi(g\mathbf{k} - \mathbf{k}), \quad (8)$$

where ‘ \equiv ’ signifies identity to within an integer. Since Φ_g , Φ'_g and χ are linear on the lattice, one finds (by substituting $\mathbf{k} = \mathbf{k}_0$) the transformation behavior of the linear and constant part of the phase function separately as

$$\Phi'_g(\mathbf{k} - \mathbf{k}_0) \equiv \Phi_g(\mathbf{k} - \mathbf{k}_0) + \chi([g - 1](\mathbf{k} - \mathbf{k}_0)) \quad (9)$$

$$\varphi'_g \equiv \varphi_g + \chi(g\mathbf{k}_0 - \mathbf{k}_0). \quad (10)$$

In Eq. (8), we see that the phase function is gauge invariant at all \mathbf{k} left invariant by g , since whenever $g\mathbf{k} = \mathbf{k}$ the last term $\chi(g\mathbf{k} - \mathbf{k})$ vanishes due to linearity. Similarly, the linear part $\Phi_g(\mathbf{K})$ is seen to be gauge invariant in Eq. (9), for all \mathbf{k} satisfying $[g - 1]\mathbf{k} = [g - 1]\mathbf{k}_0$. The values of $\Phi_g(\mathbf{k} - \mathbf{k}_0)$ for these \mathbf{k} determine whether g is a simple rotation (mirror) or a screw rotation (glide mirror), which can be seen by the same reasoning as in [25].

If $g, h \in G_E$, so is $gh \in G_E$, since G_E is a group. We can determine the corresponding phase function $\Phi_{gh}(\mathbf{K}) + \varphi_{gh}$ directly by

$$\begin{aligned} \Phi_{gh}(\mathbf{k} - \mathbf{k}_0) &\equiv \Phi_g(h(\mathbf{k} - \mathbf{k}_0)) + \Phi_h(\mathbf{k} - \mathbf{k}_0) \\ \varphi_{gh} &\equiv \varphi_g + \varphi_h + \Phi_g(h\mathbf{k}_0 - \mathbf{k}_0), \end{aligned} \quad (11)$$

These relations originate from the associativity $g(h\mathbf{k}) = (gh)\mathbf{k}$ in conjunction with Eq. (7).

Now that we can describe the symmetry of the field in terms of phase functions $\Phi(\mathbf{K}) + \varphi$, we turn to the intensity. Fourier transformation of Eq. (2) gives

$$I(\mathbf{K}) = \sum_{n=1}^N A_n^2 \delta^{(3)}(\mathbf{K}) + \sum_{n=2}^N \sum_{m=1}^{n-1} A_n A_m \left[e^{i\Psi_{nm}} \delta^{(3)}(\mathbf{K} - \mathbf{K}_{nm}) + e^{-i\Psi_{nm}} \delta^{(3)}(\mathbf{K} + \mathbf{K}_{nm}) \right], \quad (12)$$

with the three-dimensional Dirac delta distribution $\delta^{(3)}(\mathbf{K})$. Since the intensity $I(\mathbf{r})$ is a real and positive density, the application of RWM-methodology [20] for the description of its symmetries is straightforward here. Essentially, when substituting $I(\mathbf{K})$ for $E(\mathbf{k})$, leaving out \mathbf{k}_0 and neglecting the constant phases χ_0 and φ_g , all Eqs. (6)–(11) remain valid.

Finally, we want to emphasize the fact that the symmetries $g \in G_E$ of the field are at the same time also symmetries of the intensity pattern $g \in G_I$, where G_I denotes the point group of the intensity lattice. With the Wiener-Khinchin theorem we find

$$\begin{aligned} I(\mathbf{K}) &= \int d^3 k' E(\mathbf{k}') E^*(\mathbf{k}' - \mathbf{K}) \\ \Rightarrow I(g\mathbf{K}) &= \int d^3 k' E(\mathbf{k}') E^*(\mathbf{k}' - g\mathbf{K}) \end{aligned} \quad (13)$$

and substituting $\mathbf{k}' = g\mathbf{k}''$ yields

$$\begin{aligned} I(g\mathbf{K}) &= \int d^3 k'' E(g\mathbf{k}'') E^*(g[\mathbf{k}'' - \mathbf{K}]) \\ &\stackrel{(6)}{=} \int d^3 k'' e^{i2\pi[\Phi_g(\mathbf{k}'' - \mathbf{k}_0) - \Phi_g(\mathbf{k}'' - \mathbf{K} - \mathbf{k}_0)]} E(\mathbf{k}'') E^*(\mathbf{k}'' - \mathbf{K}) \\ &= e^{i2\pi\Phi_g(\mathbf{K})} \int d^3 k'' E(\mathbf{k}'') E^*(\mathbf{k}'' - \mathbf{K}) \\ \Rightarrow I(g\mathbf{K}) &\stackrel{(13)}{=} e^{i2\pi\Phi_g(\mathbf{K})} I(\mathbf{K}). \end{aligned} \quad (14)$$

In Eq. (14) we have the equivalent of Eq. (7), only for the intensity. Thus, to make sure the intensity features a given symmetry, it is enough to impose the symmetry constraints on the Fourier components of the complex field. The inverse however is not true in general: not every symmetry g of the intensity is also a symmetry of the field.

4. Periodic phase vortex lattices

Considering the interesting features and prospects of shaped vortices [26] on the one hand (e.g. in soliton dynamics [27, 28], ultracold atoms [29] or optical tweezers [30–34]), and those of nondiffracting beams [35] (e.g. in nano-processing [36] or microscopy [37]) on the other hand, it is appropriate to investigate the feasibility of nondiffracting lattices with periodically aligned optical vortices. In particular, structured arrangements of high symmetry such as on a regular lattice seem particularly attractive. Hence, we will construct triangular, hexagonal, and square vortex lattices, using the comprehensive framework introduced in Sections 2 and 3.

4.1. Lattices of triangular vortices

In the following, we are constructing a triangular vortex lattice as sketched in Fig. 2(a). It should have at least threefold symmetry and triangular domains of high intensity with a central dip (at V and W), confined by lines of zero intensity M , M' and M'' .

These lines can be realized by a mirror symmetry m : if the field's reflection at the line M (or respectively at M' or M'') is equal to the original field phase-shifted by π , we have a π -phase jump at the mirror line M (or M' , M'') and consequently the intensity will vanish there. Placing phase vortices at V and W will result in the desired central intensity dips, but because of the imposed mirror symmetry, the vortices at V must have the sign of their topological charge opposite to those at W , thus restraining rotational symmetry at R , V , or W to a threefold axis r_3 . The point group of the field is thus $G_E = \{e, r_3, r_3^2, m, m' = mr_3, m'' = r_3m\}$ (with e being the identity).

Now that the needed symmetry elements are established, we can discuss the placement of the Fourier components of the field (cf. Fig. 2(b)). The lattice is hexagonal; consequently, the wave vectors of the participating plane waves have to be located at the points of intersection of such a lattice with a circle centered around a point of three- or sixfold symmetry of the lattice, due to the desired threefold rotational symmetry r_3 . Different choices are possible (e.g. circles A , B and C in Fig. 2(b)), but one can show that the simplest configuration resulting in the point group G_E corresponds to the circle C . In A the mirror m cannot have a π -phase jump, whereas in B , the π -phase jump mirror m is incompatible with the existence of vortices.

Circle C yields six points of intersection with the lattice and knowing the directions $\mathbf{k}_0, \dots, \mathbf{k}_5$

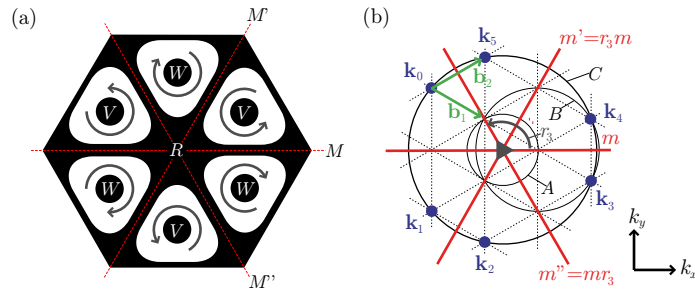


Fig. 2. (a) Desired schematic real space field distribution. (b) Basic field configurations resulting in a threefold rotational symmetry of the complex field.

of the interfering plane waves, their relative phases ψ_n and amplitudes A_n are the only unknowns left. By symmetry, all amplitudes have to be equal. The phases can be constructed by arbitrarily choosing $\psi_0 = 0$ and applying the mirror symmetry m and rotation r_3 in Fourier space. Defining the real space origin to be in the point of highest symmetry R , the phase function of the mirror m is determined by $\Phi_m(\mathbf{k} - \mathbf{k}_0) = 0$ as well as $\varphi_m = 1/2$ and the phase function of the rotation r_3 is zero: $\Phi_{r_3}(\mathbf{k} - \mathbf{k}_0) = 0$, $\varphi_{r_3} = 0$. One obtains

$$\begin{aligned}\psi_1 &= \underbrace{\psi_0}_{=0} + 2\pi(\underbrace{\Phi_m(\mathbf{k}_1 - \mathbf{k}_0)}_{=0} + \underbrace{\varphi_m}_{=1/2}) = \pi, \\ \psi_2 &= \underbrace{\psi_0}_{=0} + 2\pi(\underbrace{\Phi_{r_3}(\mathbf{k}_2 - \mathbf{k}_0)}_{=0} + \underbrace{\varphi_{r_3}}_{=0}) = 0, \\ \psi_3 &= \underbrace{\psi_1}_{=\pi} + 2\pi(\underbrace{\Phi_{r_3}(\mathbf{k}_3 - \mathbf{k}_0)}_{=0} + \underbrace{\varphi_{r_3}}_{=0}) = \pi, \\ \psi_4 &= \underbrace{\psi_2}_{=0} + 2\pi(\underbrace{\Phi_{r_3}(\mathbf{k}_4 - \mathbf{k}_0)}_{=0} + \underbrace{\varphi_{r_3}}_{=0}) = 0, \\ \psi_5 &= \underbrace{\psi_3}_{=\pi} + 2\pi(\underbrace{\Phi_{r_3}(\mathbf{k}_5 - \mathbf{k}_0)}_{=0} + \underbrace{\varphi_{r_3}}_{=0}) = \pi.\end{aligned}$$

Thus, the total field can be expressed in polar coordinates as

$$E_{\text{tri}}(\theta, r) = \sum_{n=0}^2 \left[e^{ik^\perp r \cos(\theta + \frac{2\pi n}{3} + \arctan(3\sqrt{3}))} + e^{ik^\perp r \cos(\theta + \frac{2\pi n}{3} - \arctan(3\sqrt{3})) + i\pi} \right]. \quad (15)$$

The actual field and phase distribution in real space will be shown in Section 5, together with a corresponding experimental realization.

4.2. Square vortex lattice

As in the case of the triangular vortices, we can proceed to construct a nondiffracting beam of square vortices. The lattice we are looking for is sketched schematically in Fig. 3(a).

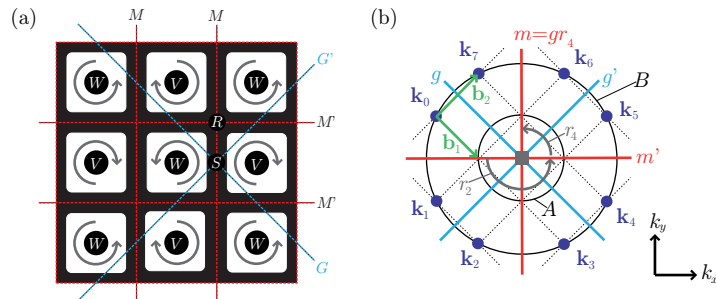


Fig. 3. (a) Desired schematic real space field distribution. (b) Basic field configurations resulting in a fourfold rotational symmetry of the complex field.

It consists of quadratic areas of high intensity with a central dip (at V and W), separated by lines of zero intensity M and M' . A vortex at V and W will give rise to the local dips, and as before, the lines of zero intensity can be realized by a π -shifting mirror, resulting in a different sign of the topological charge of the vortices at V and W . This means, that the lattice is additionally invariant under the action of the essential glide mirrors (i.e. there is no simple mirror symmetry parallel to it in real space, cf. [38]), diagonally along G and G' . Furthermore,

one notices a fourfold rotational symmetry about V and W , while only a twofold rotation r_2 is possible in R , due to the different signs of the vortices at V and W . The point group of the desired lattice thus has to contain a fourfold rotation r_4 (about V or W), a mirror m (along M or M') and a glide mirror g , g' (along G or G' respectively). Fortunately, we will see that a simple mirror m together with a diagonal glide mirror g is sufficient to generate all of the above symmetry elements.

In the next step, we have to answer the question of the location of the participating wave vectors in Fourier space. The two most basic configurations are depicted in Fig. 3(b). They are constructed by the cuts of circles A or B with a square lattice. Symmetry dictates that these circles have to be respectively centered at either of the two fourfold symmetry points of the lattice. The configuration using A however does not allow for a π -phase shifting mirror and a glide mirror at 45° to it at the same time. It turns out that a configuration using circle B is the simplest choice of plane waves, compatible with the symmetries we require, and that the π -phase jump mirror m as well as the glide mirror g have to be aligned as indicated in Fig. 3(b). Interchanging them would be incompatible with the fourfold rotational symmetry.

Now, that we have established the positioning of the plane waves, we can construct their relative phases ψ_0, \dots, ψ_7 using the phase functions corresponding to the symmetries g and m . We start again by setting $\psi_0 = 0$ and positioning the origin of real space at point S (cf. Fig. 3(a)), which is invariant with respect to mirror symmetry over G , G' and M . Consequently, the phase function of the mirror m needs to be constant in this gauge and this constant has to be $\phi_m = 1/2$, since we want a π -phase jump at the mirror planes of M . The phase functions of the glide mirror g is

$$\Phi_g(n_1\mathbf{b}_1 + n_2\mathbf{b}_2) + \varphi_g = \frac{n_1}{2} + 0 = \frac{n_1}{2}.$$

Here, the value of the constant part φ_g is obtained by application of Eq. (11) on the identity $e = gg$. One finds that either $\varphi_g = 0$ or $\varphi_g = 1/2$, both of which are valid choices. For simplicity, we opt for $\varphi_g = 0$. The form of the linear term $n_1/2$ is due to the fact, that g is an essential glide mirror (for details see [25]). In applying the phase functions of m and g to the phase ψ_0 of the plane wave at \mathbf{k}_0 we find

$$\begin{aligned} \psi_7 &= \underbrace{\psi_0}_{=0} + 2\pi(\underbrace{\Phi_g(\mathbf{b}_2)}_{=0} + \underbrace{\varphi_g}_{=0}) = 0, \\ \psi_6 &= \underbrace{\psi_7}_{=0} + 2\pi(\underbrace{\Phi_m(\mathbf{b}_1 + 2\mathbf{b}_2)}_{=0} + \underbrace{\varphi_m}_{=1/2}) = \pi, \\ \psi_1 &= \underbrace{\psi_6}_{=\pi} + 2\pi(\underbrace{\Phi_g(\mathbf{b}_1 - \mathbf{b}_2)}_{=1/2} + \underbrace{\varphi_g}_{=0}) = 2\pi \equiv 0 \bmod 2\pi, \\ \psi_4 &= \underbrace{\psi_1}_{=0} + 2\pi(\underbrace{\Phi_m(3\mathbf{b}_1 + \mathbf{b}_2)}_{=0} + \underbrace{\varphi_m}_{=1/2}) = \pi, \\ \psi_3 &= \underbrace{\psi_4}_{=\pi} + 2\pi(\underbrace{\Phi_g(3\mathbf{b}_1)}_{=1/2} + \underbrace{\varphi_g}_{=0}) = 2\pi \equiv 0 \bmod 2\pi, \\ \psi_2 &= \underbrace{\psi_3}_{=0} + 2\pi(\underbrace{\Phi_m(2\mathbf{b}_1 - \mathbf{b}_2)}_{=0} + \underbrace{\varphi_m}_{=1/2}) = \pi, \\ \psi_5 &= \underbrace{\psi_2}_{=\pi} + 2\pi(\underbrace{\Phi_g(2\mathbf{b}_1 + 2\mathbf{b}_2)}_{=0} + \underbrace{\varphi_g}_{=0}) = 0. \end{aligned}$$

All of the amplitudes A_n evidently need to be equal by symmetry here and thus, the total field

can be written as

$$E_{\text{square}}(\theta, r) = \sum_{n=0}^3 \left[e^{ik^\perp r \cos(\theta + \frac{n\pi}{2} + \arctan 2) + i\frac{n\pi}{2}} + e^{ik^\perp r \cos(\theta + \frac{n\pi}{2} - \arctan 2) + i\frac{(n+2)\pi}{2}} \right], \quad (16)$$

which is gauge equivalent to the phase configuration derived above. An experimental realization of this vortex lattice will be presented in Section 5.

4.3. Hexagonal vortices

The remaining hexagonal vortex tiling whose construction we present here in detail is sketched in Fig. 4(a). Requiring a vortex of topological charge +1 to be on the points of sixfold rotational symmetry V , the most basic configuration possible obviously consists of six plane waves along the directions $\mathbf{k}_0, \dots, \mathbf{k}_5$ whose transverse wave vectors are on the corners of a regular hexagon in Fourier space (cf. Fig. 4(b)). Rotation of the complex field by an angle of $\pi/3$ about one vortex V has to be accompanied with a constant overall phase offset of the same amount of $\pi/3$ because we requested a topological charge of 1. In Fourier space, this amounts to phases of $\psi_n = n\pi/3$.

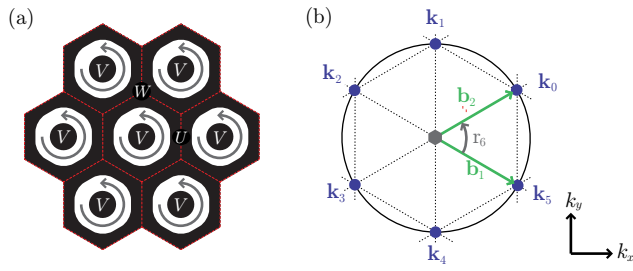


Fig. 4. (a) Desired schematic real space field distribution. (b) Most basic field configuration resulting in a sixfold rotational symmetry of the complex field.

In this case the symmetry group is solely generated by the sixfold rotation r_6 and comprises no mirror symmetries, making this – in contrast to the two vortex lattices discussed before – a chiral periodic light field. This absence of mirrors is due to the fact, that there are phase vortices on every mirror line of the underlying hexagonal lattice, breaking the mirror symmetry.

Finally, the total field can be cast into the simple form

$$E_{\text{hex}}(\theta, r) = \sum_{n=0}^5 e^{ik^\perp r \cos(\theta - \frac{\pi n}{3}) + i\frac{\pi n}{3}}. \quad (17)$$

A closer examination of the corresponding intensity and phase distributions will be given in the following Section, when discussing our experimental realization.

5. Experimental realization of all three vortex lattices

The experimental setup for the creation and analysis of the discussed nondiffracting vortex beams is shown in Fig. 5.

The continuous-wave 532nm laser beam is first cleaned of undesired spatial frequencies using a combination of microscope objective and pinhole and afterwards – to get a good approximation of a plane wave – expanded and collimated. Using a polarizing beam splitter the beam is then divided into a lattice beam and a phase reference beam. The latter can be blocked

by a shutter and is only used to determine the generated phase distribution. The other beam is led onto a phase-only spatial light modulator, which is programmed with the phase pattern $\arg(E(\mathbf{r}))$ of the desired wave field $E(\mathbf{r})$. Another spatial filtering is performed in the Fourier plane of a subsequent demagnifying telescope. The Fourier mask is a metallic plate with small holes drilled in the positions of the desired Fourier components. The size of the holes is chosen such that the sharp foci of the individual spatial frequency components can pass through them without cutoff.

The analysis of the field is performed by two measurements. First, the intensity in the region of interest is captured directly using a microscope objective and a camera. Then, in a second step, the phase distribution of the field is determined through a measurement of the Stokes parameters of the superposition of the lattice beam with the perpendicularly polarized broad phase reference. The polarization state is measured with a rotatable quarter-wave plate and a subsequent fixed polarizer using the procedure described in [39]. Thus, our setup allows for a determination of the entire complex field distribution in one transverse plane, and – mounting the imaging equipment on a translational stage – can be used for three-dimensional mapping as well.

In Fig. 6 we summarize our measurements of all three vortex lattices that were constructed in Section 4. First, we present the triangular vortex lattice in Fig. 6(a), synthesized using the Fourier components given for reference in the first column of Fig. 6(a). In the second and third column, a juxtaposition of numerically calculated and experimentally measured intensity distribution is presented. A good agreement is seen here, as well as for the numerically and experimentally obtained phases (fourth and fifth column, respectively).

Also for the lattice of quadratic vortices (Fig. 6(b)), the experimentally captured images fit the numerics very well. The rings of high intensity are distinctly separated and show a pronounced, but very localized dip at their center. An analysis of the corresponding phase images corroborates that this is indeed due to vortices and π -phase jumps at the corresponding positions.

In the case of the hexagonal vortices shown in Fig. 6(c), an evaluation of the phase pattern (fourth and fifth column) substantiates that the vortices at the center of the rings of high intensity indeed all have the same topological charge.

These experiments demonstrate thoroughly that the presented method of lattice construction is feasible and that the framework developed in Section 3 has important applications. Essen-

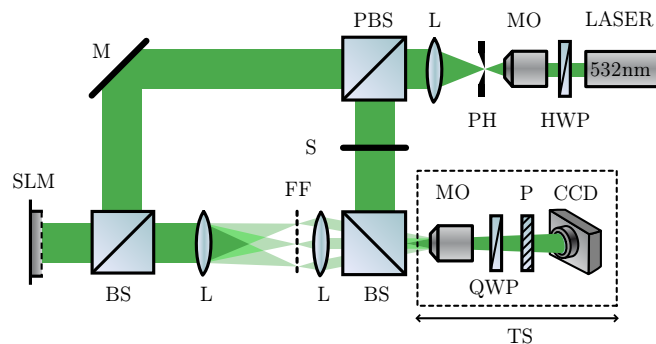


Fig. 5. Setup for the generation of the discussed lattices. BS: beam splitter, CCD: camera, L: lens, FF: Fourier filter, HWP: half-wave plate, M: mirror, MO: microscope objective, P: polarizer, PBS: polarizing beam splitter, PH: pinhole, QWP: quarter-wave plate, S: shutter, SLM: spatial light modulator, TS: translational stage.

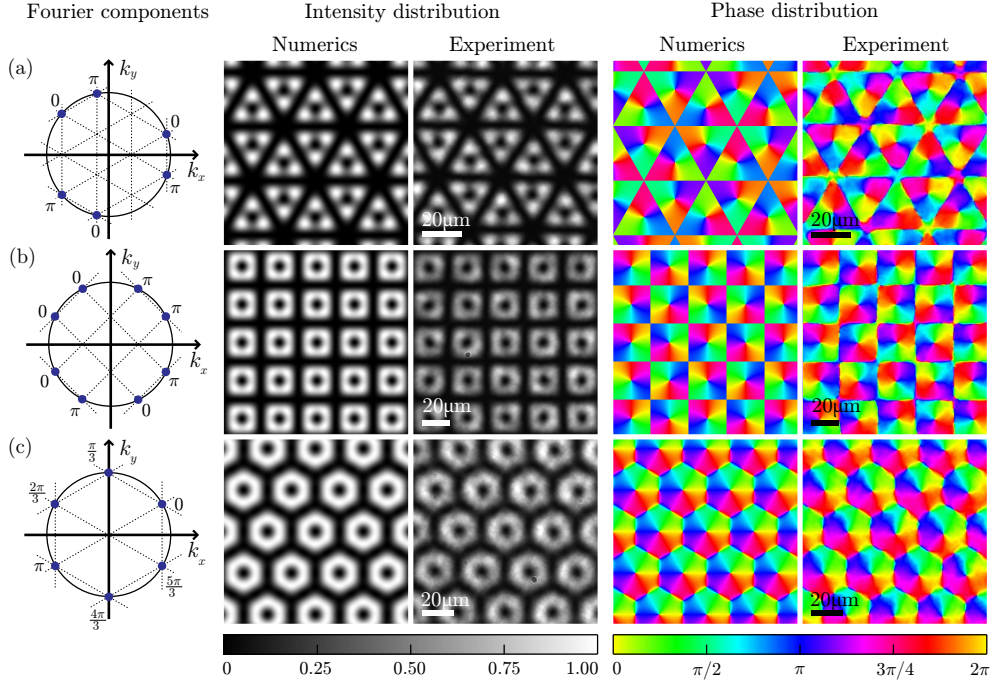


Fig. 6. Periodic nondiffracting vortex beams. First column: Transverse Fourier components of the field. Second and third column: Numerically calculated and experimentally measured intensity distributions. Fourth and fifth column: Numerically calculated and experimentally measured phase distributions.

tially, this constitutes the first systematic presentation of all three fundamental vortex lattices.

6. Three-dimensional helix lattices

The two-dimensional nondiffracting lattices of the previous section can be extruded into three-dimensional ones, by bringing them into interference with another plane wave of different k -component in the direction of the optical axis (here along the z -axis) [40]. Hereby, the phase singularity lines of the vortices are effectively transformed into screw axes having helices of high intensity around them.

6.1. Triangular helix lattice

First, we consider the lattice of triangular vortices from Fig. 6(a), which – adding a central plane wave of the same wavelength propagating in the direction of the z -axis – forms the structure depicted in Fig. 7. The total field now reads

$$E_{\text{tri,3D}}(\theta, r, z) = E_{\text{tri}}(\theta, r)e^{ik\parallel z} + A_{\text{tri}}e^{ikz}, \quad (18)$$

with A_{tri} being the amplitude of the plane wave in arbitrary units.

A good choice is the square root of the maximum intensity of the two-dimensional distribution

$$A_{\text{tri}} = \max_{\mathbf{r} \in \mathbb{R}^3} \sqrt{I_{\text{tri}}(\mathbf{r})}.$$

Here, this evaluates numerically to $A_{\text{tri}} \approx 4.39$. By interference with the additional plane wave, the lattice gains another dimension of periodicity. In real space, the corresponding period is

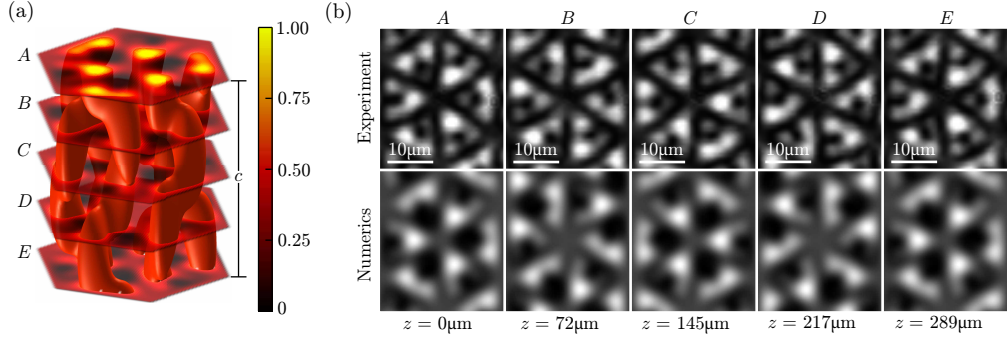


Fig. 7. Three-dimensional triangular helix lattice with longitudinal periodicity c . (a) Numerically calculated $0.6I_{\max}$ -isointensity surfaces with the slices A–E corresponding to different z -planes. (b) Comparison between numerical and experimental intensity distributions at different z .

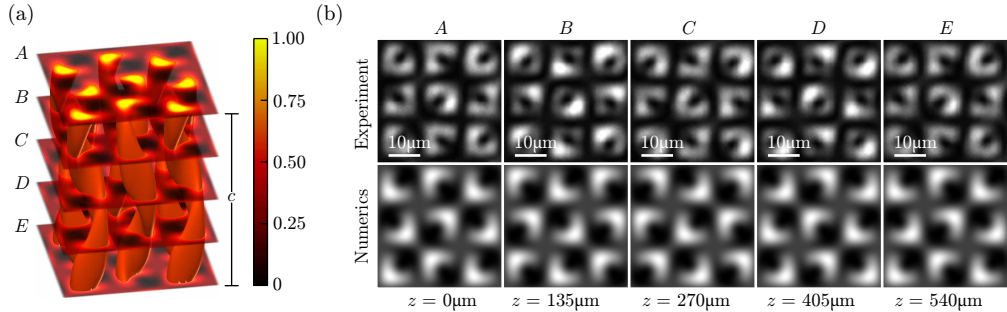


Fig. 8. Three-dimensional square helix lattice with longitudinal periodicity c . (a) Numerically calculated $0.6I_{\max}$ -isointensity surfaces with the slices A–E corresponding to different z -planes. (b) Comparison between numerical and experimental intensity distributions at different z .

$c = \lambda/(k - k^{\parallel})$ along the z -direction, with $k^{\parallel} = \sqrt{k^2 - (k^{\perp})^2}$. In Fig. 7(a), we see the $0.6I_{\max}$ -isointensity surfaces of the three-dimensional lattice. One notices, that the intensity now forms helices around 3_1 -screw axes. The fact that adjacent helices turn in opposite senses corresponds to the vortices of the field E_{tri} having topological charges with opposite signs. Despite the presence of screw axes, this configuration is still achiral because the added plane wave is on the invariant plane of the mirror symmetry of E_{tri} . Accordingly, the mirror is retained.

Figure 7(a) is equipped with several equidistant slices A–E along the z -direction, at which in Fig. 7(b) we present a comparison between the corresponding numerically calculated and experimental captured intensities. The obvious conformity between numerics and experiment proves the spiraling character of the experimentally obtained three-dimensional intensity distribution.

6.2. Square helix lattice

A similar analysis applies to the square vortex lattice from Fig. 6(b). Adding another central plane wave yields

$$E_{\text{square},3\text{D}}(\theta, r, z) = E_{\text{square}}(\theta, r) e^{ik^{\parallel}z} + A_{\text{square}} e^{ikz} \quad (19)$$

for the total field, where $A_{\text{square}} \approx 4.34$ is the optimal amplitude of the added plane wave. The resulting numerically calculated three-dimensional intensity distribution is presented in Fig. 8(a). It consists of helically shaped regions of highest intensity, arranged on a square lattice. Each individual spiral is seen to be cleanly separated from its next neighbors by planes of zero intensity parallel to the z -axis. Again, we find that adjacent helices turn in opposite senses as required by the different signs of the topological charges of the corresponding two-dimensional vortex lattice E_{square} . The modulation of the intensity along the z -axis is also recognized in the experimentally generated intensity lattice depicted in Fig. 8(b). One observes that the intensity in the plane A matches very well the intensity in E . This is due to the fact that these planes are separated by one longitudinal period c along the z -axis.

Using this intensity distribution in holographic lithography, samples with attractive properties are to be expected since it has been established – for example – that in a combination of metallic helices with different chiralities, pure magnetic or electric resonances can be selectively excited using linearly polarized light, leading to negative permittivity and negative permeability, respectively [41].

6.3. Hexagonal helix lattice

Finally, considering the hexagonal configuration in Fig. 6(c), we expect its three-dimensional extension,

$$E_{\text{hex},3D}(\theta, r, z) = E_{\text{hex}}(\theta, r)e^{ik\parallel z} + A_{\text{hex}}e^{ikz}, \quad (20)$$

with $A_{\text{hex}} \approx 3.52$ to be particularly interesting. Its intensity distribution is depicted in Fig. 9(a).

The intensity forms helices as in the two other cases considered above. But in contrast to those, the helices here all have the same rotational sense. This is expected, because already for the two-dimensional field E_{hex} the topological charges of all corresponding vortices have the same sign. Despite the absence of mirrors, each individual helix is still seen to be quite separate from its neighbors (cf. Fig. 9(b)). The origin of this is seen by a closer examination of the phase pattern of E_{hex} (cf. Fig. 6(c)) revealing additional vortices positioned at the edges and corners of the underlying hexagonal tiling (cf. U and W in Fig. 3(a)). The absence of mirror symmetries in conjunction with the helices all turning in the same sense proves the chirality of this structure, making it at the same time highly attractive for the fabrication of chiral photonic crystals or photonic lattices with fascinating properties.

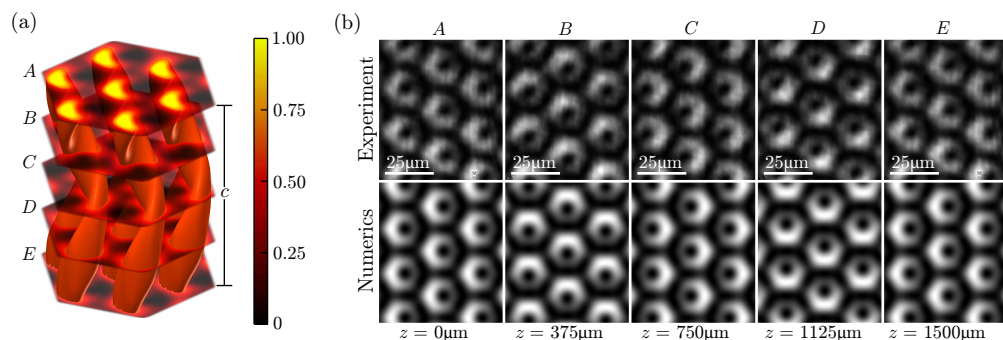


Fig. 9. Three-dimensional hexagonal helix lattice with longitudinal periodicity c . (a) Numerically calculated $0.6I_{\max}$ -isointensity surfaces with the slices $A-E$ corresponding to different z -planes. (b) Comparison between numerical and experimental intensity distributions at different z .

7. Conclusion

In conclusion, we demonstrated how the RWM-methodology for the description of symmetries in Fourier space can be generalized to include complex fields. We showed that this is a nifty tool set for the construction of periodic light fields with desired symmetry elements. More particularly, the strength of this framework was revealed by its application to the design of nondiffracting regular lattices with vortices of triangular, quadratic, and hexagonal shape.

Furthermore, we have given an extension of these lattices into three-dimensional ones, consisting of periodic arrangements of high-intensity helices in chiral and achiral configurations. Both, the two-dimensional as well as the three-dimensional lattices have successfully been implemented experimentally and demonstrated to exhibit great potential as far as the production of photonic crystal structures and metamaterials is concerned. Hence, this work constitutes the first systematic approach to the fundamental nondiffracting vortex and complex intensity helix lattices and in particular the hexagonal helix lattice was found to be valuable for the holographic lithography of chiral metamaterials.

Acknowledgments

We acknowledge support by Deutsche Forschungsgemeinschaft and Open Access Publication Fund of University of Münster.